ELSEVIER

Journal of Chromatography A, 943 (2002) 251–261

JOURNAL OF CHROMATOGRAPHY A

www.elsevier.com/locate/chroma

Characterisation of core-shell latexes by flow field-flow fractionation with multi-angle light scattering detection

Wijbren Frankema, Michel van Bruijnsvoort, Robert Tijssen, Wim Th. Kok*

Polymer-Analysis Group, Department of Chemical Engineering, University of Amsterdam, Nieuwe Achtergracht 166, 1018 WV Amsterdam, The Netherlands

Received 21 August 2001; received in revised form 26 October 2001; accepted 26 October 2001

Abstract

Flat channel asymmetrical flow field-flow fractionation with multi-angle light scattering (MALS) detection was used to study the swelling behaviour of core-shell particles with either carboxylated or hydroxylated shells as a function of pH and ionic strength. The equilibration time of the most heavily carboxylated core-shells appeared to be of the order of several hours. At low ionic strength (5 m*M*), the carboxylated core-shells showed a definite swelling response to a change in pH in the range from 5 to 10, ranging from a hydrodynamic radius increase of 24 to 118%, depending on the degree of carboxylation. A much milder response was found for the change of the root mean square (r.m.s.) radius as measured with MALS, indicating that the scattering plane is moving inwards during the swelling process due to a decreasing density of the shell. The hydroxylated core-shells appeared to be inert to a change in pH. Also the response of two expanded (pH 10) carboxylated core-shells on increasing ionic strength was studied. Comparison of the results of these ionic strength experiments with theoretical predictions based on Donnan equilibrium led us to the conclusion that a significant amount of counter-ion condensation may take place in the shells.

Keywords: Flow field-flow fractionation; Multi-angle light scattering; Core-shell latexes

1. Introduction

The visco-elastic properties of paints and coatings are of major importance with regard to their application characteristics, such as levelling out of brush or roller marks. Due to their special rheological behaviour, core-shell particles play an important role in tuning these properties for water-borne coatings (latex paints), because the shells can swell or shrink as a response to a change of environmental conditions, such as pH and ionic strength [1,2]. For acidic (e.g., carboxylated) gels, the mechanism underlying this swelling behaviour was believed to have its origin in the electrostatic repulsion between likewise charged groups [3,4], but it is well accepted now that the physical dimensions of a polymer gel are set by a balance between osmotic pressure and polymer elasticity [5–8]. In uncharged gels this osmotic pressure arises from the configurational entropy of the polymer chains, while in polyelectrolyte gels the main contribution to the osmotic pressure comes from the translational entropy of free ions in the gel [6]. In the latter case, a Donnan equilibrium requires a higher concentration of free

*Corresponding author. Tel.: +31-20-5256-539; fax: +31-20-5256-638.

E-mail address: wkok@science.uva.nl (W.T. Kok).

0021-9673/02/$ – see front matter
PII: S0021-9673(01)01460-1

ions in the gel and thus leads to an increase of the osmotic pressure, which causes the gel to swell [5]. The time constant of the swelling process has been shown to be very variable, depending on the size and composition of the gel, and the environmental conditions, such as the buffer capacity [9,10].

The subject of this study is to investigate the suitability of flow field-flow fractionation (FlFFF), coupled to a multi-angle light scattering (MALS) detector, for the characterisation of core-shell particles and their swelling behaviour.

1.1. Field-flow fractionation

Field-flow fractionation is a family of analytical separation techniques, pioneered by Giddings in 1966 [11], and has been extensively reviewed recently [12–14]. Basically, all FFF methods use two fields: an axial flow field that takes care of the elution of the components through a tapered rectangular or trapezoidal flat channel and a cross-field, perpendicular to the axial field, forcing the components toward one of the channel walls, the collection wall. The cross-field, which may be any field that is able to interact with the components, determines the sub-class of the FFF techniques. For example, we can distinguish flow FFF (FlFFF), thermal FFF (ThFFF), sedimentation FFF (SdFFF), magnetic FFF (MFFF), etc., in which the cross field is established by a cross flow, a thermal gradient, a (artificial) gravitational field or a magnetic gradient, respectively.

In the steady-state situation, the force on the analytes due to the cross-field is compensated by diffusional forces in the opposite direction, resulting in a Boltzmann distribution with the centre of mass at a distance l from the collection wall. Generally, l is expressed relative to the channel width (w) as a dimensionless parameter describing the fractional height of a sample band within the channel:

$$\lambda = \frac{l}{w} \tag{1}$$

If an error in α up to 10% is acceptable [15], the retention ratio, relating the retention time (t_R) to the void time (t_0), may be expressed as:

$$R \equiv \frac{t_0}{t_R} = 6\lambda \tag{2}$$

for $R \leq 0.5$.

For FlFFF, λ can be expressed in operational variables [15]:

$$\lambda = \frac{DV_0}{F_c w^2} \tag{3}$$

where V_0 is the channel void volume, F_c is the cross-flow rate and D is the diffusion coefficient of the analyte. Obviously, the diffusion coefficient is the only analyte property that governs retention in this case. Within the validity regime of Eq. (2), we arrive via the Stokes–Einstein equation (for spherical particles):

$$D = \frac{kT}{6\pi\eta r_H} \tag{4}$$

where k is the Boltzmann constant, T the absolute temperature, η the viscosity of the solvent and r_H the hydrodynamic radius of the particle, at:

$$r_H = \frac{kTV_0 t_R}{\pi\eta F_c w^2 t_0} \tag{5}$$

So, particle size is a linear function of retention time and can be readily calculated from the experimental FlFFF data.

The above sketched situation is valid as long as the diffusion factor is significant compared to the lateral force on the particles. However, at very high cross-fields and/or with large particles (low D), the particle motion towards the wall is not halted by diffusion anymore, but by physical contact with the collection wall [12–17]. The distribution of the particles is then determined by the particle size only, the smaller particles slipping through the interstitial space between the larger particles, and thus moving closer to the collection wall. If this is the predominant mechanism, the elution order will be reversed: the larger particles eluting faster than the smaller ones. This is called the steric mode of FFF and is, in principle, possible for all sub-classes of field-flow fractionation. In the case of normal mode FFF of particles, these steric effects should always be taken account of. Giddings [15] showed that, in

order to account for the above mentioned effects, Eq. (2) should be written as:

$$R = 6\alpha + R(\lambda) \quad (6)$$

where α is defined as:

$$\alpha \equiv \frac{r_H}{w} \quad (7)$$

With Eqs. (3) and (4) this results in a corrected expression for the particle size:

$$r_H = \frac{1}{12} \cdot \left(Rw + \sqrt{R^2 w^2 - \frac{24kTV_0}{\pi \eta V_c w}} \right) \quad (8)$$

Note that only steric effects are considered here, and that other hydrodynamic artefacts, such as lift forces [18,19], are not included.

1.2. FFF of core-shell particles

Combinations of different FFF techniques for the characterisation of core-shell particles have been reported. Ratanathanawongs and co-workers [20,21] combined either SdFFF and FlFFF or FlFFF and ThFFF, both with UV detection, for a detailed study of the behaviour of core-shell particles with a carboxylated shell. Moon et al. studied core-shell particles with a poly(L-lactide) shell with FlFFF in hyperlayer mode and UV detection [22]. Asymmetrical FlFFF and photon correlation spectroscopy (PCS) has been used by Othegraven et al. [23] to characterise fluorocarbon cores with highly cross-linked polystyrene shells. Karlsson et al. studied the swelling behaviour of carboxylated core-shell latexes with SdFFF and PCS [24].

Recently, Mes et al. [25] studied the swelling properties of carboxylated core-shell latexes with ThFFF/MALS, combined with PCS. This study showed that the use of a MALS detector, combined with a size-separation method, gives, apart from particle size, valuable extra information. However, the retention behaviour in a ThFFF channel strongly depends on the chemical composition of the particles and the eluent, which makes it hard to draw conclusions about the absolute particle size from the retention data alone. FlFFF does not have this problem because in this case the only analyte property that influences retention is the diffusion coefficient, and thus particle size.

2. Experimental

2.1. Instrumental

The FlFFF equipment used was a flat channel type FFF cell by ConSenxus (Ober-Hilbersheim, Germany). A trapezoidal channel with a length of 286 mm, an inlet width of 21.2 mm and an outlet width of 4.7 mm, was cut out of Mylar spacer with a nominal thickness of 350 μm, giving a channel volume of approximately 0.75 ml. The collection wall was a regenerated cellulose ultra-filtration membrane, with a cut-off of M_r 30 000 (C030F, Celgard, Wiesbaden, Germany). Solvent and sample delivery pumps were a Constametric 3200 (TSP, Riviera Beach, FL, USA) and a MicroStar K100 (Knauer, Berlin, Germany) pump, respectively. Sample injection was performed with a Rheodyne 7010 six-way injection valve (Berkeley, CA, USA) and a 20 μl loop. Cross-flows were monitored and controlled with a series L30 LiquiFlow mass flow meter/controller (Bronkhorst High-Tech, Ruurlo, The Netherlands).

Detection systems were a Spectroflow 757 UV detector (Applied Biosystems, Ramsey, NJ, USA) and a DAWN-DSP MALS detector (Wyatt Technology, Santa Barbara, CA, USA), equipped with a 30 mW argon ion laser (488 nm) [26].

2.2. Samples

The core-shell samples were kindly provided by AKZO (Arnhem, The Netherlands) as dispersions in water. Table 1 lists the definitions and the reported properties of the samples. Before injection, all latexes were diluted 1:5000 in the appropriate buffer solution to a final concentration of approximately 40 μg/ml.

2.3. Chemicals

Mobile phases were prepared from 2 m*M* Tris buffer (pH values 7 to 10) or benzoate buffer (pH values 5 and 6) and adjusted to the desired ionic

Table 1
Summary of sample properties as provided by AKZO (Arnhem, The Netherlands)

Sample code	Core used	Core composition (%, w/w)		Shell composition (%, w/w)				OH/acid composition (mmol/g)
		BMA	Sty	BAA	MMA	MAA	HEMA	
Core1	–	80	20	–	–	–	–	0
Core2	–	80	20	–	–	–	–	0
Carb1	Core1	80	20	34.4	61.3	4.3	–	0.5
Carb2	Core2	80	20	36.6	52.6	10.8	–	1.25
Carb3	Core1	80	20	38.8	44	17.2	–	2
OH1	Core1	80	20	31.6	61.7	–	6.5	0.5
OH2	Core2	80	20	29.5	54.1	–	16.3	1.25
OH3	Core2	80	20	27.5	46.4	–	26.2	2

For convenience the original sample codes have been replaced for the ones in the first column. MAA: methacrylic acid, BMA: butylmethacrylate, Sty: styrene, BA: butylacrylate, MMA: methylmethacrylate, HEMA: hydroxyethylmethacrylate. The fifth column (OH/acid) gives the base concentration of the shell in case of the OH samples, or the acid concentration of the shell in case of the Carb samples.

strength with sodium chloride. The mobile phases also contained 300 mg/l Brij 35 (Acros Organics, NJ, USA) to reduce adsorption of the particles to the collection wall. All solutions were prepared with sub-boiled water and filtered over a 0.45 μm HV filter (Millipore, Bedford, MA, USA).

Calibration of the MALS detector was done with toluene (99+, Acros Organics, NJ, USA), filtered twice over a 20 nm Anodisc 47 filter (Whatman, Maidstone, UK). Normalisation of the MALS was done with Pullulan P-20 standard ($M_w = 23\,700$, $M_w/M_n = 1.07$, Polymer Labs., Amherst, MA, USA), which is reported to have a Stokes diameter of 9 nm in water [27].

The FFF focusing point was checked with bromophenol blue (BDH, Poole, UK) and calibration of the FFF channel was performed with type I horse spleen ferritin (Sigma, St. Louis, MO, USA).

All chemicals not explicitly specified were analytical grade and obtained from standard suppliers.

2.4. Procedures

The position and shape of the FFF focusing point was visually inspected by injecting 2 mg/ml bromophenol blue, which was made basic by the addition of a few drops of 0.1 *M* NaOH. The calibration of the FFF channel was performed by the injection of 1 mg/ml ferritin. From the retention data, determined from the UV signal at 280 nm, the height (w) of the channel was calculated according to the procedure described by Litzén [28]. The eluent during this calibration procedure was 5 m*M* NaCl solution. The channel was judged to be well assembled if complete resolution of the ferritin monomer and dimer could be obtained.

The fractionations were performed in three steps. After an initial stabilisation time of 10 s, the sample was injected during 50 s at 0.15 ml/min. Then, relaxation and focusing was carried out during a pre-established time (visual inspection with bromophenol blue), long enough for the sample to concentrate in a narrow band of about 1 mm thickness, at a total flow-rate, equal to that during elution, immediately followed by the elution phase, in which the eluted sample was continuously monitored successively by the UV detector (254 nm for the core-shell latexes) and the MALS detector. After completion of the run, the channel was rinsed for another 5 min with zero cross-flow.

Diffusion coefficients were calculated according to Litzén [29,30]. In order to get accurate results at low retention a numerical solution for the exact expression for R was used in these cases. The results were corrected for steric foldback according to Eq. (6). Hydrodynamic diameters were obtained from the diffusion coefficients via the Stokes–Einstein equation for spherical particles.

MALS detection was carried out with 11 detectors, at scattering angles from 30 to 150°. The

collected data were processed with the Astra for Windows software (Wyatt Technology, Santa Barbara, CA, USA), version 4.5, using a second-order Berry fit.

3. Results and discussion

In order to get a grasp of the relaxation of the core shells as a response to a change in pH the most carboxylated sample, i.e., Carb3, was dispersed in a pH 10 Tris buffer and the radius was monitored during 5 h. Fig. 1 shows the results of this experiment for r_H, indicating that the relaxation process takes approximately 5 h to come about. To ensure complete adaptation to the conditions of pH and ionic strength in further experiments, the samples were allowed to equilibrate in the buffer overnight (at least 12 h).

To study the importance of particle–particle and particle–wall interactions and to estimate an operating domain where these interactions are minimised, the influence of the flow conditions (cross flow velocity) on the apparent hydrodynamic radii of the particles was determined. The experiments were performed at pH 10 because this was the highest value in the experimental range with the maximum

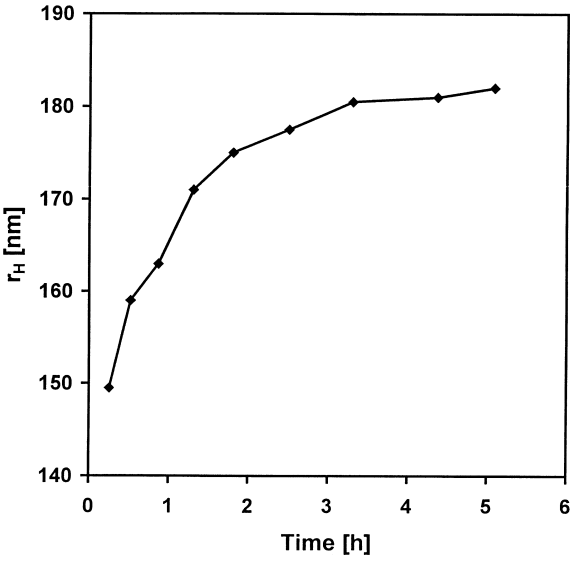

Fig. 1. Relaxation of r_H of Carb3 after dispersion of the sample in 2 m*M* Tris buffer at pH 10.

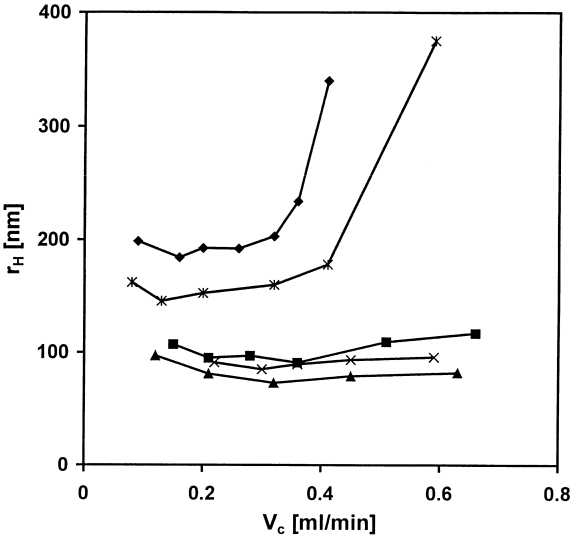

Fig. 2. Apparent hydrodynamic radius as a function of cross flow in 2 m*M* Tris buffer at pH 10 and $[Na^+]=5$ m*M*. Samples are Carb1 (■), Carb2 (∗), Carb3 (♦), OH2 (×) and Core1 (▲).

particle radii. Inter-particle and particle–wall interactions may be expected to be most pronounced at higher particle diameter. As is shown in Fig. 2, the apparent hydrodynamic radii of the most heavily carboxylated core-shells, i.e., Carb2 and Carb3, clearly increase when the cross-flow exceeds 0.3 ml/min; for Carb3 this effect is even quite dramatic. The effect on the other core-shell particles is negligible or not present at all. The r.m.s. radii for all particles, as measured with MALS, were independent of the cross-flow, indicating that the observed effect on the hydrodynamic radii of Carb2 and Carb3 has its origin in particle–particle and/or particle–wall interactions. This is further supported by the observed effect of the cross-flow on the peak symmetry.

For a full understanding of the interpretations in this article it is necessary to clearly distinguish between the different definitions for the radius. The hydrodynamic radius (r_H) is the radius of a hypothetical hard sphere that diffuses with the same speed as the particle under examination. It thus represents the size of the outer envelope of the particle. The r.m.s. radius (r_g), as obtained from the MALS data, is the mass-integrated square radius with respect to the centre of gravity, and thus depends on the mass

distribution within the particle. In MALS terminology, the r.m.s. radius is often erroneously called the radius of gyration, which is defined around an axis. For a discussion of these definitions and the origin of the confusion, see Ref. [31].

Note that during focusing the particles are most concentrated near the wall, which means that particle–particle and particle–wall interactions may be expected to be most prominent in this stage of the procedure. However, during the optimisation of the separation process, focusing conditions were chosen such, that the peak profiles were independent of the focusing conditions, indicating that the effect of focusing on these interactions is minimal.

The asymmetries of the peaks increase as a function of F_c, as is shown in Fig. 3 for Carb3 and Carb1. At low cross-flows both peaks are slightly fronting ($A_{10}<1$), but on increasing F_c we see an increase of A_{10} into the tailing domain for Carb3, where the asymmetry of the Carb1 peak remains constant. The increased adsorption may be due to direct particle–wall interaction, but also to entanglement of shells with the shells of already adsorbed particles. Also, entanglement of shells of dispersed (non-adsorbed) particles may give rise to an increase of D and so to a higher retention and tailing peaks. So, in order to get reliable results, the operational conditions for the FFF experiments on Carb2 and Carb3 should be chosen in such a way, that the cross-flow does not exceed 0.3 ml/min.

A typical example of a fractogram obtained with our FlFFF/MALS equipment is shown in Fig. 4A for Carb3. The monodispersity of the sample size is clear from the plot of the calculated r.m.s. radius. Fig. 4B shows a fractogram of OH3, which consistently appeared to have a tailing asymmetry. The inserted plot of the r.m.s. radius immediately makes

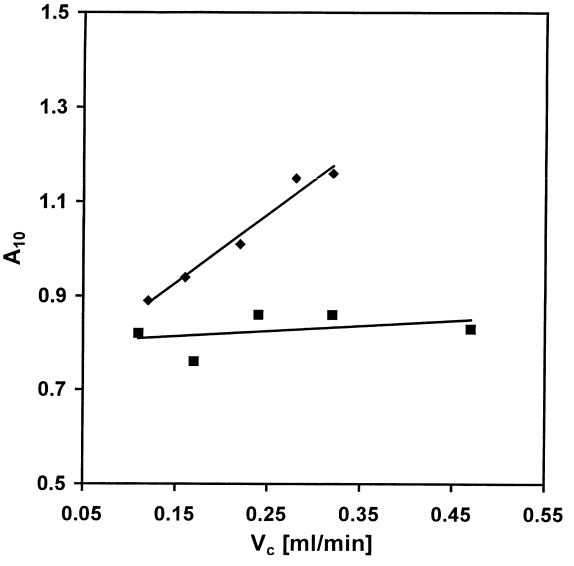

Fig. 3. The asymmetry factor measured at 10% of the peak height for Carb1 (■) and Carb3 (♦). Same conditions as in Fig. 2. The lines are linear regression lines calculated for the two data sets for guiding the eyes.

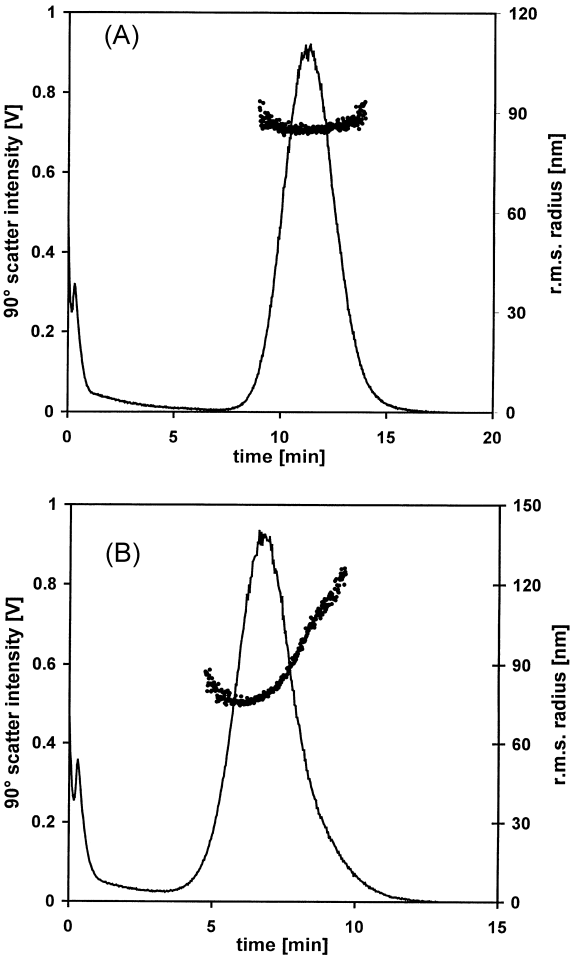

Fig. 4. Fractograms of Carb3 (A) and OH3 (B). The drawn line represents the MALS signal at a 90° scattering angle; the scatter plot shows the r.m.s. radii. Sample dilutions 1:5000. Injection volume 20 μl. V_i: 2.5 ml/min. F_c: 0.3 ml/min. Tris buffer (pH 10) with 5 m*M* ionic strength.

clear that this sample is not monodisperse, and that it actually consists of a rather monodisperse fraction and a polydisperse fraction at the higher end. From this example the power of FlFFF/MALS is evident at once.

First, the behaviour of the core-shells at different pH values at a constant ionic strength of 5 m*M* was studied. Swelling of the carboxylated core-shells on increasing pH is obvious from Fig. 5A, with the radius of the most heavily carboxylated shell (Carb3) increasing a factor 2.2 over the experimental pH range, the radius of the intermediately carboxylated shell (Carb2) increasing a factor 1.8, and that of the least carboxylated one (Carb1) increasing a factor 1.2. As a reference a 155 nm polystyrene latex standard was fractionated, which, expectedly, turned

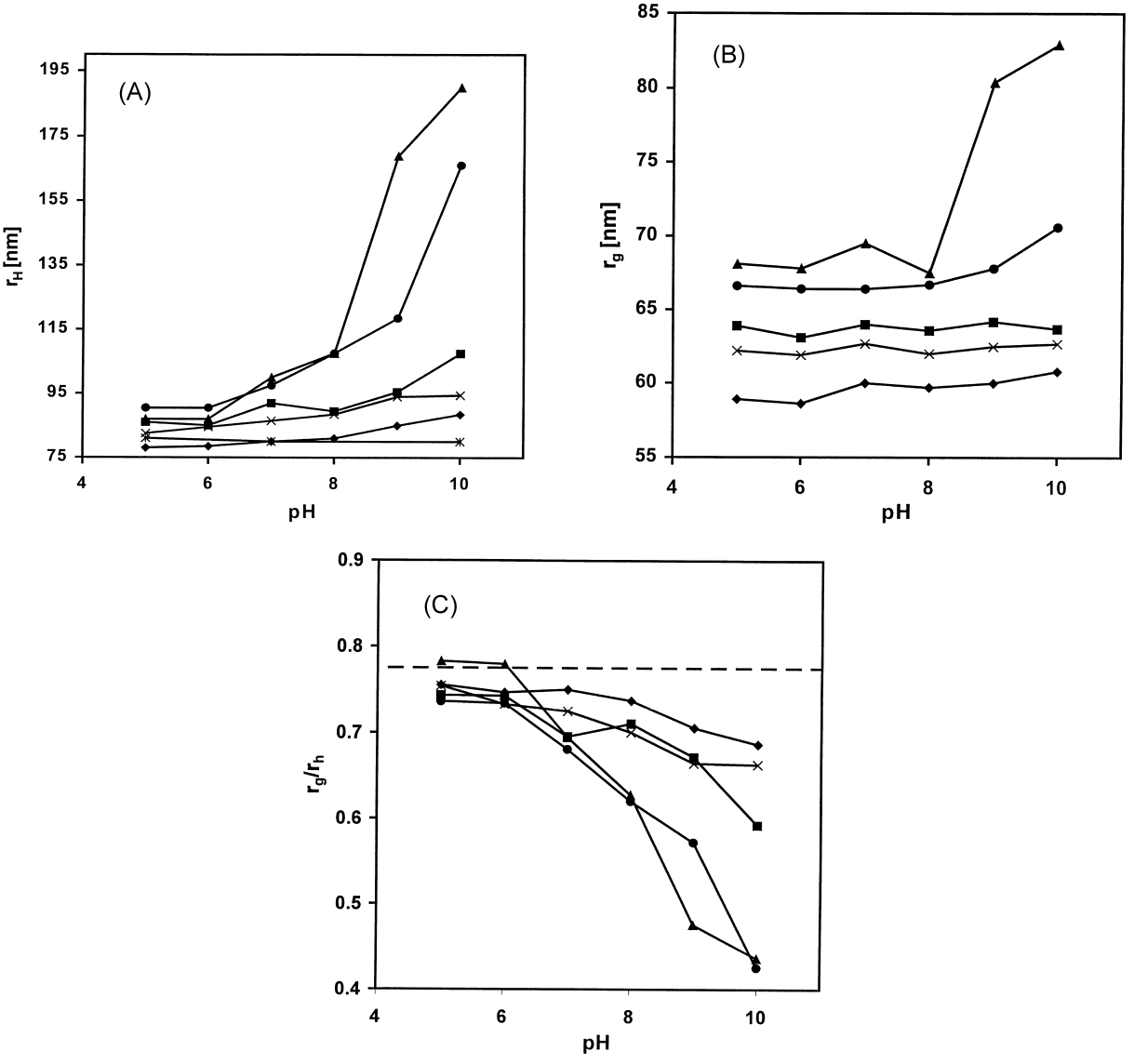

Fig. 5. Hydrodynamic radius (A), r.m.s. radius (B) and r_g/r_H ratio (C) as function of pH for Carb1 (■), Carb2 (●), Carb3 (▲), Core1 (♦), Core2 (×) and PS 155 latex standard (∗). The dashed line in (C) represents the theoretical value for dense spherical scatterers.

out to be completely inert for a change in pH. Surprisingly we also noticed a significant increase of the radius of both core particles (Core1 and Core2) with a factor 1.1 (13%). As the increase seems to start from the beginning of the pH range (acidic conditions), it is not probable that alkaline hydrolysis of the BMA ester groups are responsible for this behaviour. Probably a small fraction of the ester groups already was hydrolysed in the original material.

From the hydrodynamic radii the maximum swelling factor q_m on a volumetric basis for the shells was calculated, by comparing the shell volumes at pH 10 to those at low pH (the average of the measurements at pH 5 and pH 6). For Carb1, Carb2 and Carb3 q_m values of 3.8, 19,3 and 33.9, respectively, were found.

The swelling of the hydroxylated core-shells appeared to be much less, as is shown in Fig. 6A. The hydrodynamic radius increased with a factor 1.1 over the entire pH range, so that the effect may be completely attributed to the swelling of the core alone.

Fig. 5B shows us that the effect of pH on the r.m.s. radius, as measured by MALS, is much less then the effect on the hydrodynamic radius. The r.m.s. radius of Carb3 increased a factor 1.2 over the whole experimental pH range, while the r.m.s. radius of Carb2 only grew a factor 1.1. There was no noticeable increase of the r.m.s. radii of Carb1 and the bare core. Swelling of the particles is also reflected in the r_g/r_H ratios as depicted in Fig. 5C. At low pH values, these ratios for the carboxylated core-shells, as well as the bare cores, are close to the theoretical value for scattering spheres ($\sqrt{3/5}=0.775$). However, on increasing pH, and so on swelling, the ratio drops. For the two most carboxylated shells, Carb2 and Carb3, this effect is quite strong. To explain this, it should be realised that scattering on a particle only occurs if there is a difference in refractive index between the scattering particle and the dispersion medium. If the shell expands and absorbs more liquid from the dispersion medium, the shell density will decrease and the refractive index of the shell will more and more approach that of the medium. The result is that the scattering area moves from the surface of the shell inward toward the more dense, deeper regions.

Fig. 6B and C show the r_g and r_g/r_H data for the hydroxylated shells. As the influence of a change in pH on the hydrodynamic radii of these shells was mentioned to be marginal, it is no surprise that the r.m.s. radii are inert to a change in pH. The curves of the r_g/r_H ratio do show a significant downward trend, but also follow the curve of the bare core, implying that the swelling behaviour of the hydroxylated shells may be largely attributed to the core itself.

The experiments on the influence of the pH on the swelling behaviour of the core-shell particles as described above have been conducted at a constant ionic strength of 5 m*M*. The effect of the ionic strength of the dispersing solution on the swelling was studied at pH 10, because the swelling effects are most manifest at high pH. In Fig. 7 the results of these studies are shown for Carb1 and Carb3. It is clear that the shells condense significantly with increasing ionic strength.

The swelling behaviour of the shells of the particles can be compared with the theoretical model for swelling of polymer gels with fixed ionic groups as developed by Flory [32]. Flory derived expressions for the maximum swelling ratio of a polymeric network, based on Donnan equilibrium of ions inside and outside the gel and the network elasticity. He discerned two ionic strength regimes. In solutions with an ionic strength that is low compared to the concentration of fixed charges in the gel, the theory predicts a swelling ratio for the gel independent of the ionic strength. The maximum swelling ratio q_m is then expected to be a function of the fixed charge density c_i in the (swollen) gel only:

$$q_m \propto c_i^{\frac{3}{2}} \tag{9}$$

It is interesting to compare this prediction with the volumetric swelling ratios for the shells as calculated from the hydrodynamic radii of the carboxylated particles at an ionic strength of 5 m*M*. From the mass fraction of metacrylic acid in the shells of the three carboxylated core-shell particles, and the swelling ratio of the shells at pH 10, the concentration of ionisable groups in the shells at pH 10 could be calculated. The three-point regression line of log q_m vs. log c_i was found to have a slope of 1.63, against a predicted value of 1.5.

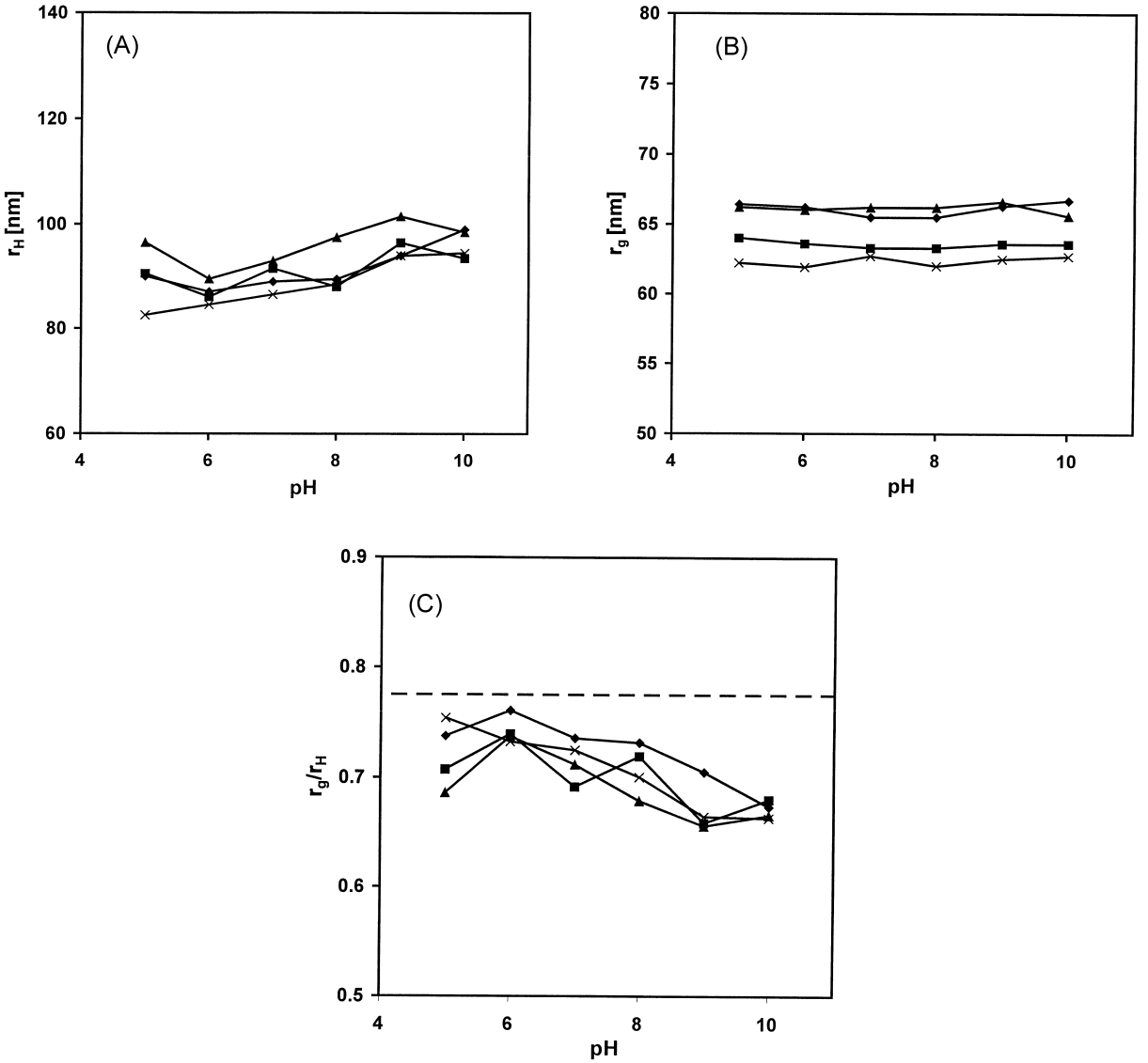

Fig. 6. Hydrodynamic radius (A), r.m.s. radius (B) and r_g/r_H ratio (C) as function of pH for OH1 (■), OH2 (▲), OH3 (♦) and Core2 (×). The dashed line in (C) represents the theoretical value for dense spherical scatterers.

The other ionic strength regime discerned by Flory is when the concentration of the fixed charges in the gel is much lower than the ionic strength I of the surrounding solution. For this regime Flory derived the expression:

$$q_m^{\frac{5}{3}} \propto \frac{c_i^2}{I} \tag{10}$$

When it is assumed that at pH 10 the ionisation of the carboxylic groups in the shells is complete, the requirements for this ionic strength regime to hold are not met under the experimental conditions of this series of experiments. Under all conditions the concentration of ionisable groups in the swollen shells is larger than, or comparable to the salt concentration in the outside solution. Still, as is shown in Fig. 7, the effect of the ionic strength on the swelling follows the trend as predicted by Eq.

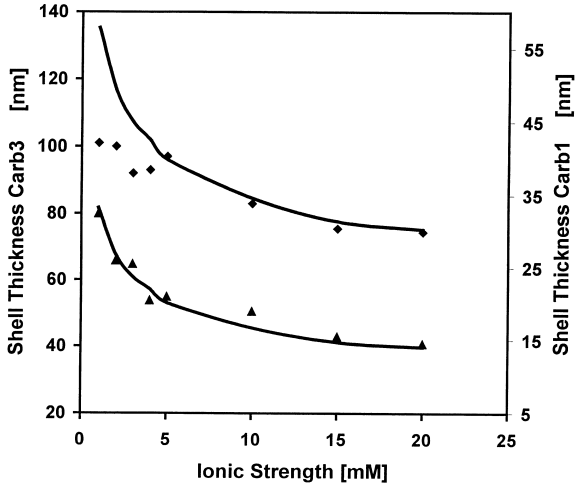

Fig. 7. Shell thickness at pH 10 as a function of the ionic strength for Carb1 (■) and Carb3 (♦). The solid lines represent predictions based on the theoretical model discussed in the text.

(10). Only at very low ionic strength a flattening of the curve for Carb3, compared to the predicted line, is seen. This, however, may be explained by the approach of the elastic limit of the polymer network. The good match between the experimentally observed swelling ratios and the theoretical prediction may be explained by counter-ion condensation. Due to the complexation of buffer (sodium) ions with the carboxyl groups of the shell material, the actual concentration of fixed ionised groups in the gel may be much lower than expected on basis of the assumption of complete ionisation. When counter-ion condensation would be significant, the conditions for Eq. (10) to hold might be met.

4. Conclusions

We have demonstrated that asymmetrical flow field-flow fractionation with MALS detection is a solid method for the characterisation of core-shell particles. When combined, the two techniques synergistically co-operate in the elucidation of the swelling behaviour of the shells. As far as the response of the core-shell particles to a change in ionic strength is concerned, the results appeared to be consistent with theoretical predictions based on Donnan equilibrium, provided that the effective degree of ionisation of the carboxylic groups is much lower than may be expected from mere acid–base considerations. The latter suggests that other factors, such as counter-ion condensation, play an important role in the swelling equilibrium. The exact nature of particle–wall and particle–particle interactions in FFF needs further investigation.

References

[1] B. Hirzinger, M. Helmstedt, J. Stejskal, Polymer 41 (2000) 2883.
[2] M.S. Wolfe, Prog. Org. Coatings 20 (1992) 487.
[3] H. Nakamura, K. Tachi, J. Appl. Polym. Sci. 65 (1997) 1933.
[4] J.R. Ford, A.A. Morfesis, R.L. Rowell, J. Colloid Interface Sci. 105 (1985) 516.
[5] G.M. Eichenbaum, P.F. Kiser, S.A. Simon, D. Needham, Macromolecules 31 (1998) 5084.
[6] M. Rubinstein, R.H. Colby, A.V. Dobrynin, J.F. Joanny, Macromolecules 29 (1996) 398.
[7] B.R. Saunders, H.M. Crowther, B. Vincent, Macromolecules 30 (1997) 482.
[8] G.M. Eichenbaum, P.F. Kiser, A.V. Dobrynin, S.A. Simon, D. Needham, Macromolecules 32 (1999) 4867.
[9] R.A. Siegel, in: K. Dusek (Ed.), Advances in Polymer Science, Vol. Trans. I, Springer-Verlag, Berlin, 1993, p. 233.
[10] G. Löhr, in: R.M. Fitch (Ed.), Proceedings of the Symposium On the Physical Chemical Properties of Colloidal Particles, Miami, FL, Polymer Colloids II, Plenum Press, 1980, p. 71.
[11] J.C. Giddings, Sep. Sci. 1 (1966) 123.
[12] M. Martin, Adv. Chromatogr. 39 (1998) 1.
[13] H. Cölfen, M. Antonietti, Adv. Polym. Sci. 150 (2000) 67.
[14] M.E. Schimpf, K.D. Caldwell, J.C. Giddings (Eds.), Field-Flow Fractionation Handbook, Wiley–Interscience, New York, 2000.
[15] J.C. Giddings, Sep. Sci. Technol. 13 (1978) 241.
[16] M.N. Myers, J.C. Giddings, Anal. Chem. 54 (1982) 2284.
[17] S. Lee, J.C. Giddings, Anal. Chem. 60 (1988) 2328.
[18] P.S. Williams, M.H. Moon, Y. Xu, J.C. Giddings, Chem. Eng. Sci. 51 (1996) 4477.
[19] P.S. Williams, M.H. Moon, J.C. Giddings, Colloids Surfaces A 113 (1996) 215.
[20] S.K. Ratanathanawongs, P.M. Shiundu, J.C. Giddings, Colloids Surfaces A 105 (1995) 243.
[21] S.K. Ratanathanawongs, J.C. Giddings, Polym. Mater. Sci. Eng. 70 (1993) 26.
[22] M.H. Moon, K. Kim, Y. Byun, D. Pyo, J. Liq. Chromatogr. Rel. Technol. 22 (1999) 2729.
[23] J. Othegraven, R. Piazza, E. Bartsch, Macromol. Symp. 151 (2000) 515.
[24] O.J. Karlsson, K.D. Caldwell, D.C. Sundberg, Macromol. Symp. 151 (2000) 503.

[25] E.P.C. Mes, W.Th. Kok, R. Tijssen, Chromatographia 53 (2001) 697.
[26] P.J. Wyatt, J. Colloid Interface Sci. 197 (1998) 9.
[27] B. Wittgren, K.G. Wahlund, J. Chromatogr. A 760 (1997) 205.
[28] A. Litzén, Anal. Chem. 65 (1993) 461.
[29] A. Litzén, J. Chromatogr. 548 (1991) 393.
[30] A. Litzén, Anal. Chem. 63 (1991) 1001.
[31] P.J. Wyatt, Anal. Chim. Acta 272 (1993) 1.
[32] P.J. Flory, Principles of Polymer Chemistry, Cornell University Press, Ithaca, NY, 1953.